Schweizerischer Erdbebendienst
Service Sismologique Suisse
Servizio Sismico Svizzero
Servizi da Terratrembels Svizzer

ETH
Eidgenössische Technische Hochschule Zürich
Swiss Federal Institute of Technology Zurich

Martigny - rue d'Octodure (SMAO)

SITE CHARACTERIZATION REPORT

Clotaire MICHEL, Daniel ROTEN, Jan BURJANEK

Valerio POGGI, Carlo CAUZZI, Donat FÄH

Sonneggstrasse 5 CH-8092 Zürich Switzerland; E-mail: clotaire.michel@sed.ethz.ch

Last modified : November 5, 2013

Abstract

Ambient vibration array measurements were performed to characterize the fluvial deposits at site Martigny Octodure. The site, where the new station SMAO of the Swiss Strong Motion Network was installed, is located on the deeply filled glacial valley of the Dranse river, adjacent to the main Rhone valley. SMAO replaces the dial-up station SMAV. In order to characterize the velocity profile under the station, array measurements with a $400\,\mathrm{m}$ aperture were performed. In addition, single station measurements showed a weak 2D behaviour of this valley. The fundamental resonance frequency is found at $0.85\,\mathrm{Hz}$. The measurements were successful and allowed deriving a velocity model for this site. The soil column underlying station SMAO is made of only $3\,\mathrm{m}$ of soft sediments, variable across the array, on top on highly consolidated sediments ($20\,\mathrm{m}$ at $700\,\mathrm{m/s}$ and $200\,\mathrm{m}$ at $1000\,\mathrm{m/s}$). An interface around $250\,\mathrm{m}$ was found (velocity above $1500\,\mathrm{m/s}$) but it cannot be assured that is corresponds to the bedrock that could be even deeper considering the geological and geomorphological indications. $V_{s,30}$ is at $570\,\mathrm{m/s}$. The ground type is B for EC8 [CEN, 2004] and SIA261 [SIA, 2003]. The theoretical SH transfer function and impedance contrast of the quarter-wavelength velocity computed from the inverted profiles show moderate amplifications at low frequencies increasing with frequency up to a factor of 5 at high frequencies. Recordings of the new station will allow to validate these simple 1D models.

Contents

1 Introduction

The station SMAO (Martigny - rue d'Octodure) is part of the Swiss Strong Motion Network (SSMNet) in the Rhone valley. SMAO has been installed in the framework of the SSMNet Renewal project in 2012 and replaces the dial-up station SMAV (Martigny - Verdan). This project includes also the site characterization. Passive array measurements have been selected as a standard tool to investigate these sites. Such a measurement campaign was carried out on 26th June 2012 around the station (Fig. 1), with a centre close to SMAO, in order to characterize the sediments under this station. According to the geological map, this station is located on a deeply filled glacial valley (Dranse river) adjacent to the main Rhone valley. In addition, a single station measurement campaign was performed across the valley of the Dranse river. This report presents the previous available data, the new measurement setup, the results of the H/V analysis and of the array processing of the surface waves (dispersion curves). Then, an inversion of these results into velocity profiles is performed. Standard parameters are derived to evaluate the amplification at this site.

Canton	City	Location	Station code	Site type	Slope
Valais	Martigny	Octodure	SMAO	Sedimentary valley	Flat

Table 1: Main characteristics of the study-site.

Figure 1: Picture of the site.

2 Experiment description

2.1 Ambient Vibrations

The ground surface is permanently subjected to ambient vibrations due to:

- natural sources (ocean and large-scale atmospheric phenomena) below $1\,\mathrm{Hz}$,
- local meteorological conditions (wind and rain) at frequencies around $1\,\mathrm{Hz}$,
- human activities (industrial machines, traffic…) at frequencies above $1\,\mathrm{Hz}$ [Bonnefoy-Claudet et al., 2006].

The objective of the measurements is to record these ambient vibrations and to use their propagation properties to infer the underground structure. First, the polarization of the recorded waves (H/V ratio) is used to derive the resonance frequencies of the soil column. Second, the arrival time delays at many different stations are used to derive the velocity of surface waves at different frequencies (dispersion). The information (H/V, dispersion curves) is then used to derive the properties of the soil column using an inversion process.

2.2 Equipment

For the single station measurement and the array measurement campaigns, 1 and 12 Quanterra Q330 dataloggers named NR01 to NR12 and 1 and 14 Lennartz 3C 5 s seismometers were available (see Tab. 2), respectively. Each datalogger can record on 2 ports, A (channels EH1, EH2, EH3 for Z, N, E directions) and B (channels EH4, EH5, EH6 for Z, N, E directions). Time synchronization was ensured by GPS. For the array measurement, the sensors were placed on a metal tripod in a $20\,\mathrm{cm}$ deep hole, when possible, for better coupling with the ground.

Digitizer	**Model**	**Number**	**Resolution**
	Quanterra Q330	1	$24\,\mathrm{bits}$
	Quanterra Q330	12	$24\,\mathrm{bits}$
Sensor type	**Model**	**Number**	**Cut-off frequency**
Velocimeter	Lennartz 3C	1	$0.2\,\mathrm{Hz}$
Velocimeter	Lennartz 3C	14	$0.2\,\mathrm{Hz}$

Table 2: Equipment used.

2.3 Geometry of the measurements

The single station measurement consisted in a cross section of 14 points from North to South (Fig. 2).

For the array measurement, two configurations were used, for a total of 4 rings of 20, 50, 100 and $200\,\mathrm{m}$ radius around a central station. The first configuration includes the 3 inner rings

with 14 sensors; the second configuration includes the 2 outer rings (plus 2 sensors of the first ring) with 13 sensors. The minimum inter-station distance and the aperture are therefore 20 and 200 m and 20 and 400 m, respectively. The experimental setup is displayed in Fig. 3.

The final usable datasets are detailed in section 3.2.

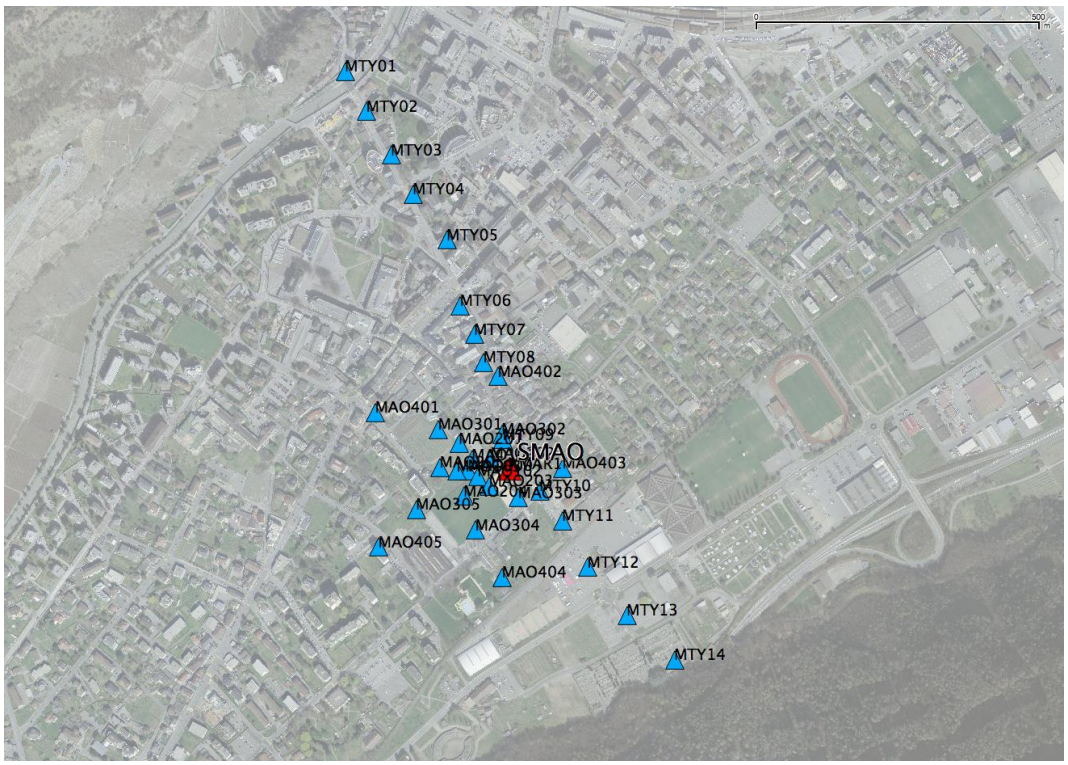

Figure 2: Position of points of both experiments.

2.4 Positioning of the stations

For the single station measurements, the points were picked on the Swisstopo aerial image, with an estimated accuracy of 2 m.

For the array, the sensor coordinates were measured using a differential GPS device (Leica Viva GS10), including only a rover station and using the Real Time Kinematic technique provided by Swisstopo. However, the GSM module did not work (wrong configuration) and only GPS raw data was written during 5 min at each point, without control on the precision. Post-processing was performed using the Leica-Geo Office software and a Virtual Reference provided by Swisstopo. It allowed an absolute positioning with an accuracy better than 5 cm on the Swissgrid except for point MAO405 with a precision of 11 cm and point MAO402 with 8 cm. This precision was assumed sufficient for this processing.

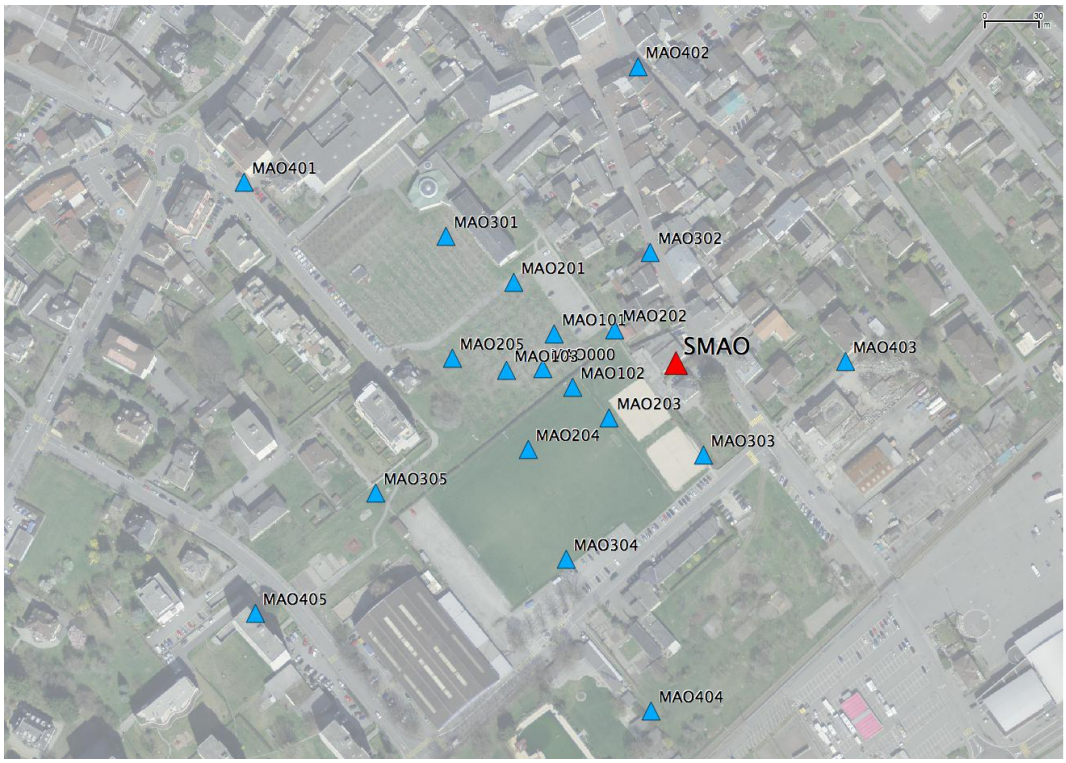

Figure 3: Geometry of the array measurement experiment.

3 Data quality

3.1 Usable data

For the single station experiment, time was not synchronized on GPS. Data is generally noisy due to the presence of pedestrians and traffic.

For the array, the largest time windows were extracted, for which all the sensors of the array were correctly placed and the GPS synchronization was ensured. The measurement was performed in the evening and during the night, the site was generally quiet, except on the sport field during the first measurement. Light showers occurred during the whole measurement time. GPS measurements, relatively long, were performed during the recordings.

A machine with a frequency of $7.13\,\mathrm{Hz}$ was running during the first dataset. Other machines were at frequencies above $15\,\mathrm{Hz}$. For the first dataset, point MAO204, MAO304 and in a lower extent MAO203 were close to people playing football and volleyball and display high amplitudes on a broad frequency range.

During the second dataset, $50\,\mathrm{Hz}$ noise is affecting several traces but it should not affect the results of the analysis. Important peaks due to soil-structure interaction are noticed at points MAO401 (2.82, 3.49 and $4.88\,\mathrm{Hz}$) and MAO405 (2.71 and $2.95\,\mathrm{Hz}$). Noise at low frequency of MAO403 is high, maybe due to coupling issues. Moreover, at some stations (MAO204, MAO301 and MAO405) the phase shift (b value of the SAC header) appears to be too large for Geopsy software to determine synchronized windows for processing (H/V, FK). The b values were therefore set to 0 in the dataset used for these computations. It does not seem to affect the results.

The characteristics of the datasets are detailed in Tab. 3.

3.2 Data processing

The data were first converted to SAC format including header entries for the point coordinates (CH1903 system), the recording component and a name related to the position. The name is made of 3 letters characterizing the location (MTY for the single station measurements, MAO for the array), and three digits. For the array, they correspond to the ring (first digit) and the number in the ring (two last digits). Recordings were not corrected for instrumental response.

Dataset	**Starting Date**	**Time**	**Length**	F_s	**Min. inter-distance**	**Aperture**	**# of points**
MTY01	2011/05/10	11:25	30 min	200 Hz			1
MTY02	2011/05/10	12:13	30 min	200 Hz			1
MTY03	2011/05/10	13:00	30 min	200 Hz			1
MTY04	2011/05/10	13:51	30 min	200 Hz			1
MTY05	2011/05/10	14:39	30 min	200 Hz			1
MTY06	2011/05/10	15:26	30 min	200 Hz			1
MTY07	2011/05/10	16:15	30 min	200 Hz			1
MTY08	2011/05/10	17:03	30 min	200 Hz			1
MTY09	2011/05/11	06:56	30 min	200 Hz			1
MTY10	2011/05/11	07:43	30 min	200 Hz			1
MTY11	2011/05/11	08:29	30 min	200 Hz			1
MTY12	2011/05/11	09:15	30 min	200 Hz			1
MTY13	2011/05/11	10:01	30 min	200 Hz			1
MTY14	2011/05/11	10:53	30 min	200 Hz			1
1	2012/06/26	16:23	124 min	200 Hz	20 m	200 m	14
2	2012/06/26	19:24	135 min	200 Hz	20 m	400 m	13

Table 3: Usable datasets.

4 H/V processing

4.1 Processing method and parameters

In order to process the H/V spectral ratios, several codes and methods were used. The classical H/V method was applied using the Geopsy `http://www.geopsy.org` software. In this method, the ratio of the smoothed Fourier Transform of selected time windows are averaged. Tukey windows (cosine taper of 5% width) of $50\,\mathrm{s}$ long overlapping by 50% were selected. Konno and Ohmachi [1998] smoothing procedure was used with a b value of 80. The classical method computed using the method of Fäh et al. [2001] was also performed.

Moreover, the time-frequency analysis method [Fäh et al., 2009] was used to estimate the ellipticity function more accurately using the Matlab code of V. Poggi, available in the software repository of the engineering seismology group of SED. In this method, the time-frequency analysis using the Wavelet transform is computed for each component. For each frequency, the maxima over time (10 per minute with at least $0.1\,\mathrm{s}$ between each) in the TFA are determined. The Horizontal to Vertical ratio of amplitudes for each maximum is then computed and statistical properties for each frequency are derived. A Cosine wavelet with parameter 9 is used. The mean of the distribution for each frequency is stored. For the sake of comparison, the time-frequency analysis of Fäh et al. [2001], based on the spectrogram, was also used, as well as the wavelet-based TFA coded in Geopsy.

The ellipticity extraction using the Capon analysis [Poggi and Fäh, 2010] as well as fundamental mode obtained using the wavefield decomposition method [Maranò et al., 2012] (see section on array analysis) were also performed.

Method	Freq. band	Win. length	Anti-trig.	Overlap	Smoothing
Standard H/V Geopsy	$0.2-20\,\mathrm{Hz}$	$50\,\mathrm{s}$	No	50%	K&O 80
Standard H/V D. Fäh	$0.2-20\,\mathrm{Hz}$	$30\,\mathrm{s}$	No	75%	-
H/V TFA Geopsy	$0.2-20\,\mathrm{Hz}$	Morlet m=8 fi=1	No	-	-
H/V TFA D. Fäh	$0.2-20\,\mathrm{Hz}$	Specgram	No	-	-
H/V TFA V. Poggi	$0.2-20\,\mathrm{Hz}$	Cosine wpar=9	No	-	No

Table 4: Methods and parameters used for the H/V processing.

4.2 Results in the array

H/V curves are consistent for all the recordings (Fig. 4). The fundamental frequency is found around $0.85\,\mathrm{Hz}$ with little variability, probably due to the quality of the recordings, and an amplitude around 4. Some of the recordings could not be picked (Fig. 4): MAO204, MAO304 and MAO403 (in red on Fig. 4). MAO203 has also a similarly strange behaviour (in orange on Fig. 4). These points were already noted as problematic concerning their quality in the previous section. MAO302, MAO303, MAO401, MAO402, MAO404 and MAO405 have lower peak values compared to the others for an unknown reason (in blue on Fig. 4). Looking at the horizontal spectra only gives the same picture with points where the peak at is clear $0.85\,\mathrm{Hz}$ and low quality spectra without clear peak. Moreover, all the methods to compute H/V ratios

are compared at the array centre on Fig. 6, in which the classical methods were divided by $\sqrt{2}$ to correct from the Love wave contribution [Fäh et al., 2001]. The classical and TFA methods match well for the right flank of the peak but the peak value is slightly different for each method. The 3C FK analysis (Capon method) does not have resolution down to the peak but matches well at frequencies above $1.3\,\mathrm{Hz}$.

Polarization analysis was performed using the code of Burjánek et al. [2010]. It shows a weak polarization in a broad frequency range including the fundamental frequency (Fig. 7). It is therefore difficult to interpret the H/V peak as a 2D or 1D mode.

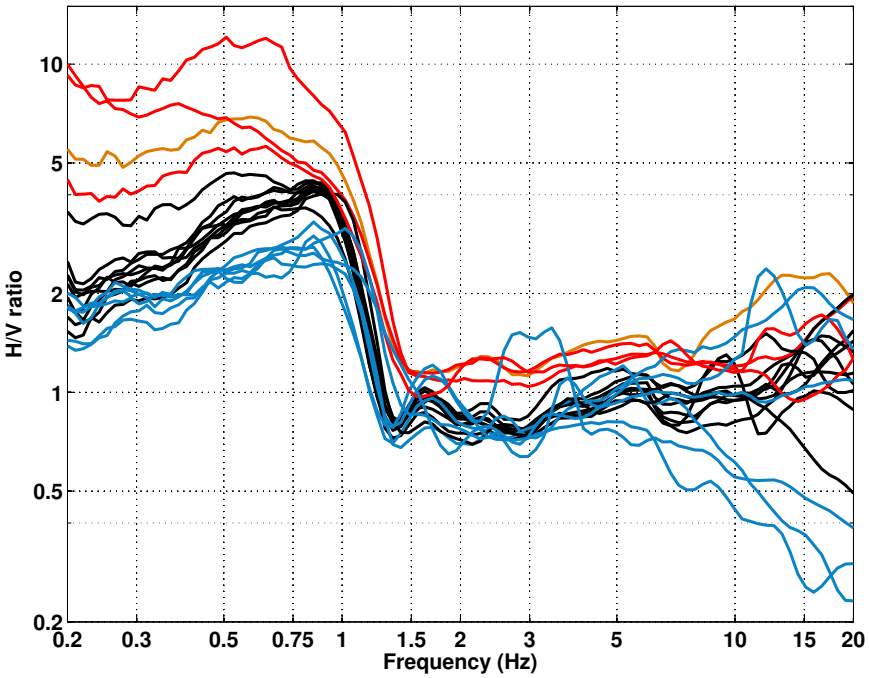

Figure 4: H/V spectral ratios (time-frequency analysis code V. Poggi). Red and orange color correspond to points with low quality recordings, blue curves have lower amplitudes.

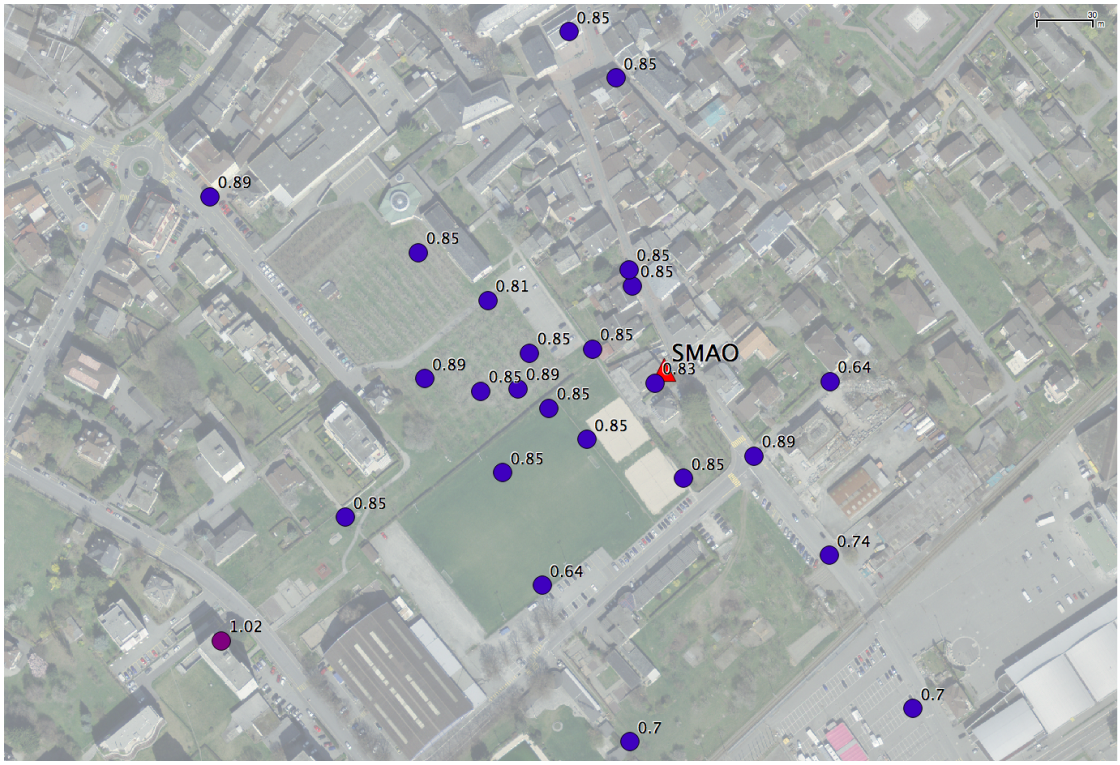

Figure 5: Map of the resonance frequencies (in Hz) within the array (code V. Poggi).

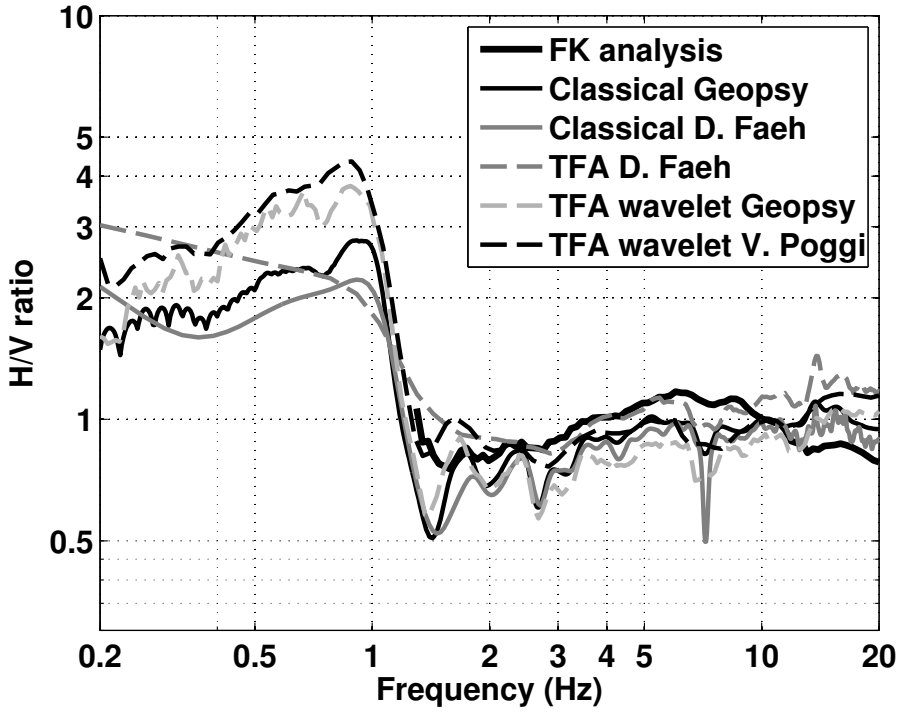

Figure 6: H/V spectral ratios for point MAO000 using the different codes. Classical methods were divided by $\sqrt{2}$.

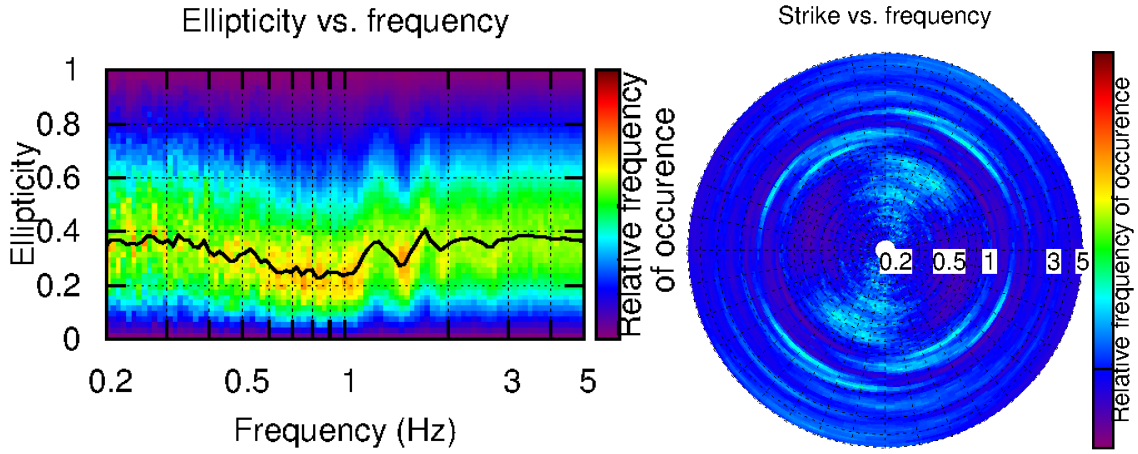

Figure 7: Polarization analysis at point MAO000. Left: Ellipticity (A trough in the ellipticity corresponds to polarized motion). Right: Strike of the polarization.

4.3 Results in the whole profile

The resonance frequency at $0.85\,\mathrm{Hz}$ can be further seen on all points in the city, even at the southern edge of the basin (not dominating) (Fig. 8). These results were obtained using the TFA methods, this peak is not so clear using only the classical H/V. Moreover, secondary peaks at higher frequencies can be seen for some points like (MTY002 and MTY003)

Figure 8: Map of the resonance frequencies (in Hz) in the city of Martigny.

5 Array processing

5.1 Processing methods and parameters

The vertical components of the arrays were processed using the FK and the High-resolution FK analysis [Capon, 1969] using the Geopsy `http://www.geopsy.org` software. Better results were obtained using large time windows (300T). The results of computations of both datasets were merged to estimate the dispersion curves.

Moreover, a 3C array analysis [Fäh et al., 2008] was also performed using the array_tool_3C software [Poggi and Fäh, 2010]. It allows to derive Rayleigh and Love modes including the Rayleigh ellipticity. The results of computations of both datasets were merged to estimate the dispersion curves.

Method	Set	Freq. band	Win. length	Anti-trig.	Overlap	Grid step	Grid size	# max.
HRFK 1C	1	$0.8 - 25\,\mathrm{Hz}$	$300T$	No	50%	0.001	0.6	5
HRFK 1C	2	$0.8 - 25\,\mathrm{Hz}$	$300T$	No	50%	0.001	0.6	5
HRFK 3C	1	$0.8 - 20\,\mathrm{Hz}$	Wav. 10	No	50%	200	3000	5
			Tap. 0.2			m/s	m/s	
HRFK 3C	2	$0.8 - 20\,\mathrm{Hz}$	Wav. 10	No	50%	200	3000	5
			Tap. 0.2			m/s	m/s	

Table 5: Methods and parameters used for the array processing.

5.2 Obtained dispersion curves

The first mode (Rayleigh) in the 1C FK analysis could be picked between 1.45 and $14.5\,\mathrm{Hz}$ (Fig. 9) including its standard deviation. The phase velocities are ranging from $1850\,\mathrm{m/s}$ at $1.45\,\mathrm{Hz}$ down to $450\,\mathrm{m/s}$ at $14.5\,\mathrm{Hz}$. Moreover, a difference of about 10% in velocity can be noticed between dataset 1 and 2 (dataset 1 faster). It is probably due to lateral variability of the upper layers. Since roman ruins were found in the central part of the array, the foundation soil was probably stiffer than the surroundings (external ring of the array). The first Rayleigh higher mode can also be picked on a short frequency band.

Using the 3C analysis, both fundamental Rayleigh and Love modes can be picked (Fig. 9). The fundamental Rayleigh mode is similar to the 1C analysis (Fig. 10). It is picked from 1.4 to $20\,\mathrm{Hz}$ and the Love mode is picked from 2 to $13\,\mathrm{Hz}$ (Fig. 10). The confidence in the low frequency part of the Love mode is limited.

The comparison (Fig. 11) with the array performed close to the SSMNet dial-up station SMAV in 2006 [Roten, 2007], with a centre located $1\,\mathrm{km}$ towards W, at the basin edge, shows a different Rayleigh dispersion curve. The strong velocity increase in these curves, corresponding to the bedrock, is at higher frequency at SMAV, corresponding to a bedrock present at shallower depth, which is awaited. Moreover, it shows lower velocities in the sediments.

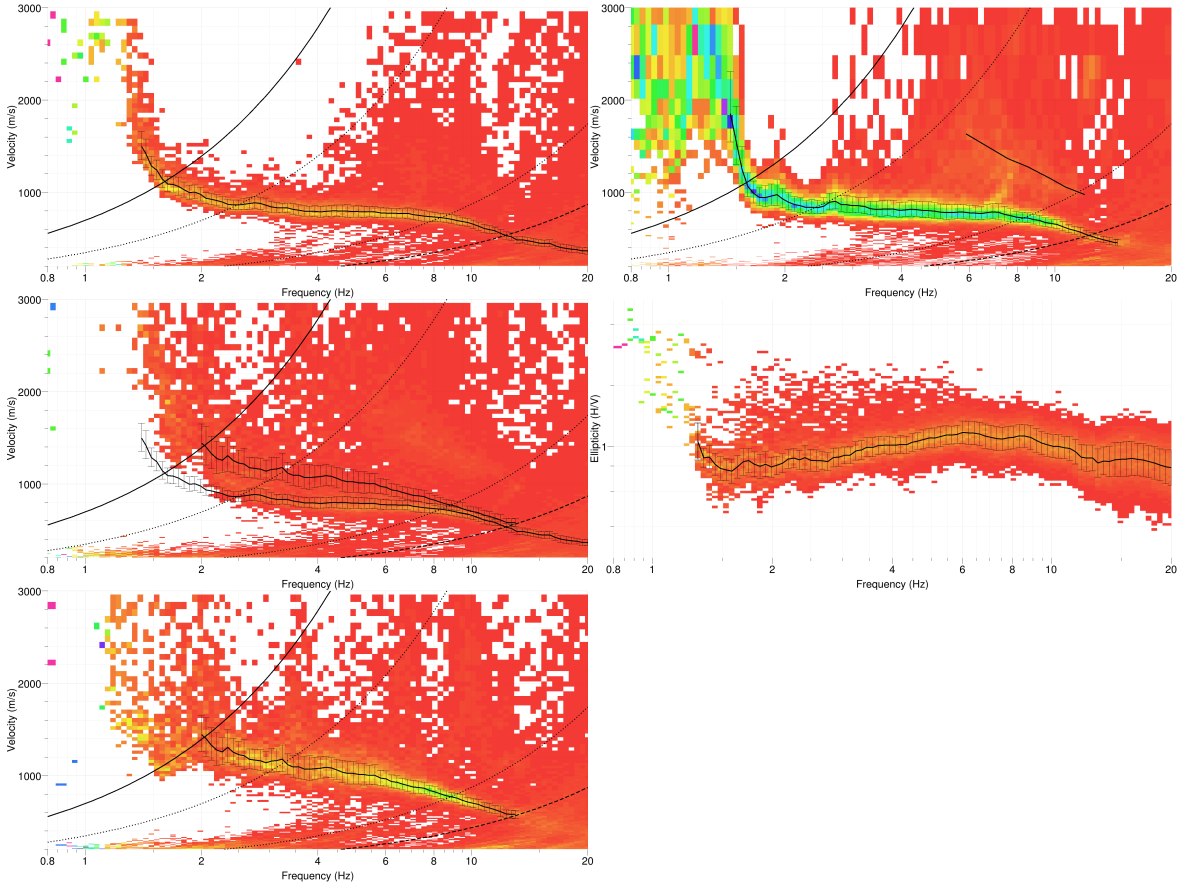

Figure 9: Dispersion curves obtained from the 3C (left) and 1C (top right) array analysis (top: vertical; centre: radial; bottom: transverse components) and ellipticity from 3C analysis (centre right).

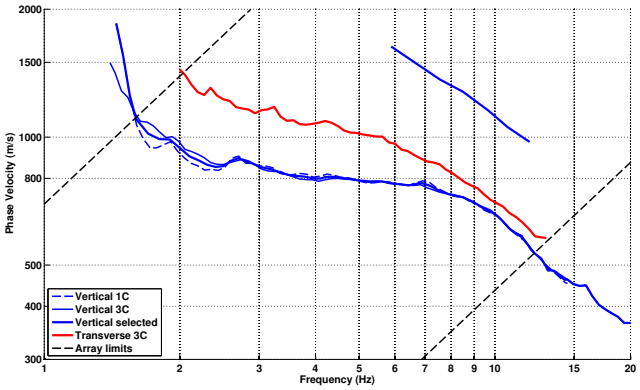

Figure 10: Picked dispersion curves from 1C and 3C FK methods.

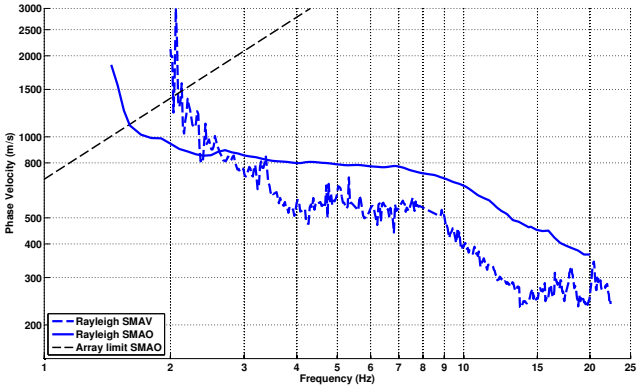

Figure 11: Comparison between Rayleigh dispersion curves in stations SMAO and SMAV.

6 Inversion and interpretation

6.1 Inversion

For the inversion, Rayleigh and Love fundamental modes dispersion curves and Rayleigh higher mode (without standard deviation to avoid different weighting) were used as simultaneous targets. All curves were resampled using 50 points between 0.6 and $20\,\mathrm{Hz}$ in log scale. The higher mode is considered to be the second higher mode. Inversion of the Love fundamental mode was limited to the frequency band $8 - 13\,\mathrm{Hz}$, because no model could be found that matches the picked Love dispersion curve. It can be seen on Fig. 9 that the Love dispersion curve is smeared at frequencies below $8\,\mathrm{Hz}$, probably due to the fact that fundamental and higher modes are mixed. The ellipticity was not used in the inversion because of the 2D resonance. It happens not to be necessary to find the bedrock interface.

The inversion was performed using the Improved Neighborhood Algorithm (NA) Wathelet [2008] implemented in the Dinver software. In this algorithm, the tuning parameters are the following: Ns_0 is the number of starting models, randomly distributed in the parameter space, Nr is the the number of best cells considered around these Ns_0 models, Ns is the number of new cells generated in the neighborhood of the Nr cells (Ns/Nr per cell) and It_{max} is the number of iteration of this process. The process ends with $Ns_0 + Nr * \frac{Ns}{Nr} * It_{max}$ models. The used parameters are detailed in Tab. 6.

It_{max}	Ns_0	Ns	Nr
500	10000	100	100

Table 6: Tuning parameters of Neighborhood Algorithm.

During the inversion process, low velocity zones were not allowed. The Poisson ratio was inverted in each layer in the range 0.2-0.4, up to 0.47 where the water table may be located. The density was supposed equal to $2000\,\mathrm{kg/m^3}$ except for the layers assumed to be rock ($2500\,\mathrm{kg/m^3}$). Inversions with free layer depths as well as fixed layer depths were performed. 4 layers are enough to explain most of the targets, but more layers are used to smooth the obtained results and better explore the parameter space. 5 independent runs of 5 different parametrization schemes (5 and 6 layers over a half space and 11, 13 and 16 layers with fixed depth) were performed. For further elaborations, the best models of these 25 runs were selected (Fig. 15).

According to the free layer depth inversion, the first layer is $3\,\mathrm{m}$ deep with a velocity between 160 and $200\,\mathrm{m/s}$. The first layer is underlain by a unit with a shear-wave velocity of $700\,\mathrm{m/s}$ that extends down to $20\,\mathrm{m}$ depth. Below $20\,\mathrm{m}$ depth a homogeneous layer with with Vs between 900 and $1000\,\mathrm{m/s}$ is encountered that extends down to an interface located between 220 and $260\,\mathrm{m}$ depth, where velocities increase to more than $1500\,\mathrm{m/s}$. The two first velocity contrasts should create peaks above $10\,\mathrm{Hz}$ that cannot be clearly seen in the H/V measurements. The deepest velocity contrast is producing a peak around $1\,\mathrm{Hz}$. It is consistent with the 2D resonance peak (at $0.85\,\mathrm{Hz}$ considering that we may not be at the deepest part of the basin) which would not bring additional valuable information in the inversion. Moreover, the models show a large peak in the H/V curve at $15 - 20\,\mathrm{Hz}$ due to the first $3\,\mathrm{m}$ of soft sediments. This peak is not seen on all the H/V curves indicating it is probably variable across the array.

When comparing to the target curves (Fig. 13 and Fig. 14), all curves, imposing a heavy constraint, are well represented. The ellipticity, that is not used in the inversion, makes somehow sense, except the high frequency peak.

According to Rosselli (2004), who developed a model of the quaternary sediments depth in the Rhone valley, the bedrock at this site is located at about $100\,\mathrm{m}$ depth. However, the Rhone basin is very deep close to Martigny (down to $900\,\mathrm{m}$), and therefore the bedrock is very steep. Assuming the bedrock slope is constant below the sediments compared to the surrounding slopes ($40\,^{\circ}$), one can estimate that the sediment thickness is about $400\,\mathrm{m}$. The gravimetry inversion seems therefore unrealistic at this site, maybe due to the level of compaction of the sediments, which seems quite high. It is not clear whether the inversion of these array measurement was able to resolve the bedrock, but this measurement is not able to provide information from larger depth. The sediments below $3\,\mathrm{m}$ depth can already be considered as rock from the engineering point of view (compacted gravels?). This site can be compared to the Chur site, where very stiff sediments were also found (alluvial fan from a mountain river made of gravels), despite of a deep sedimentary basin, as well as the Bramois site near Sion [Roten et al., 2008].

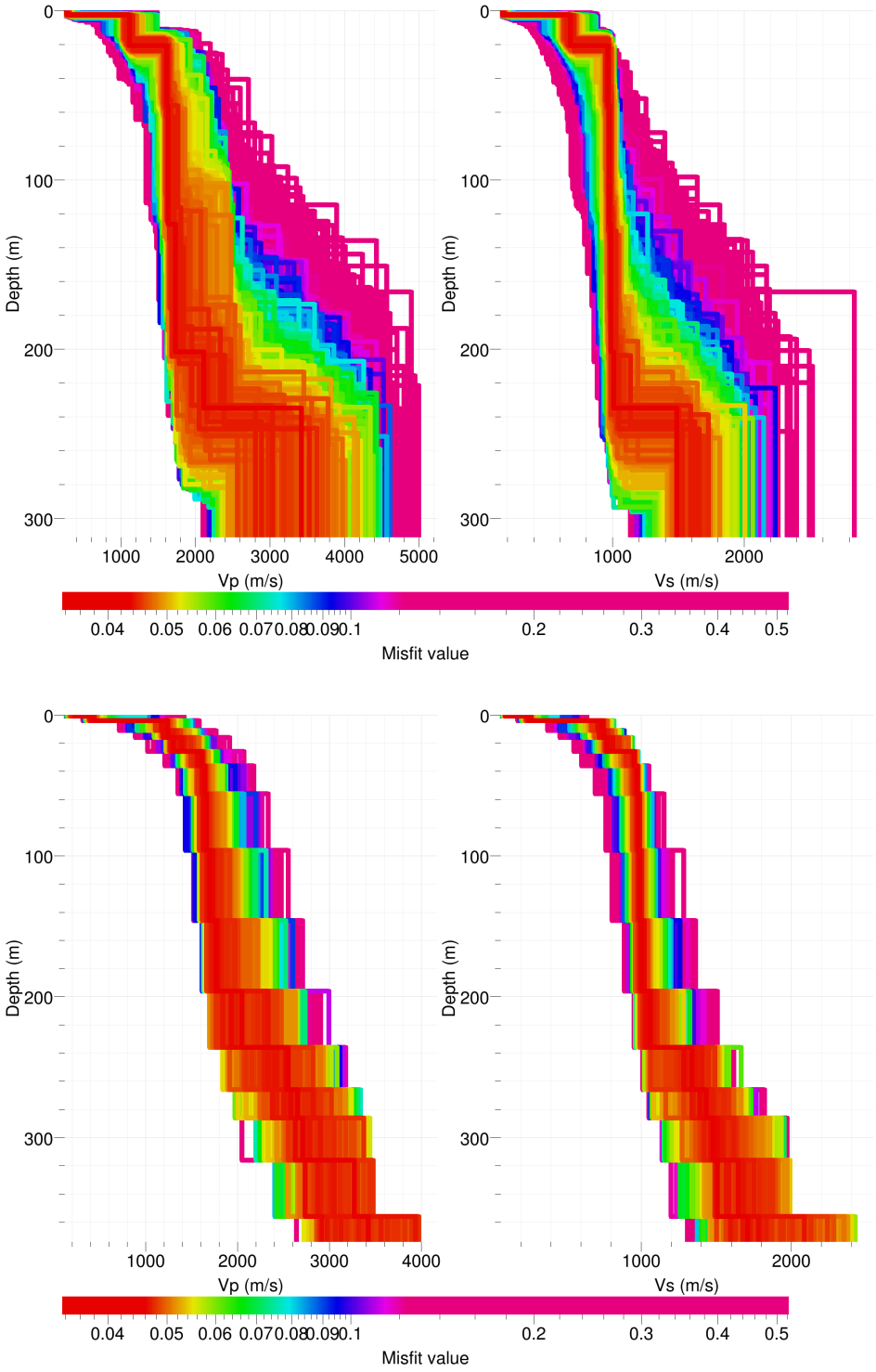

Figure 12: Inverted ground profiles in terms of V_p and V_s; top: free layer depth strategy; bottom: fixed layer depth strategy.

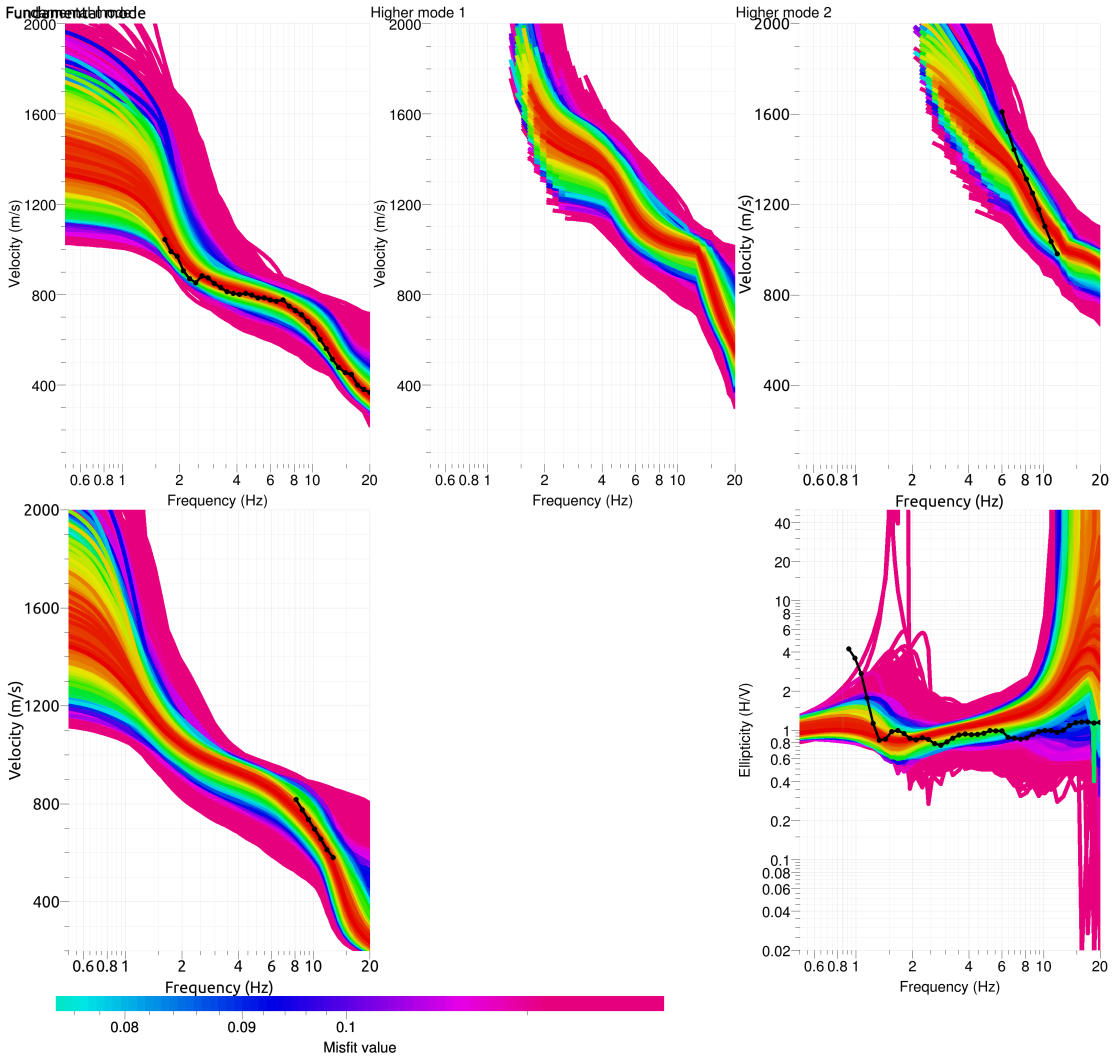

Figure 13: Comparison between inverted models and measured Rayleigh and Love modes and corresponding ellipticity, free layer depth strategy.

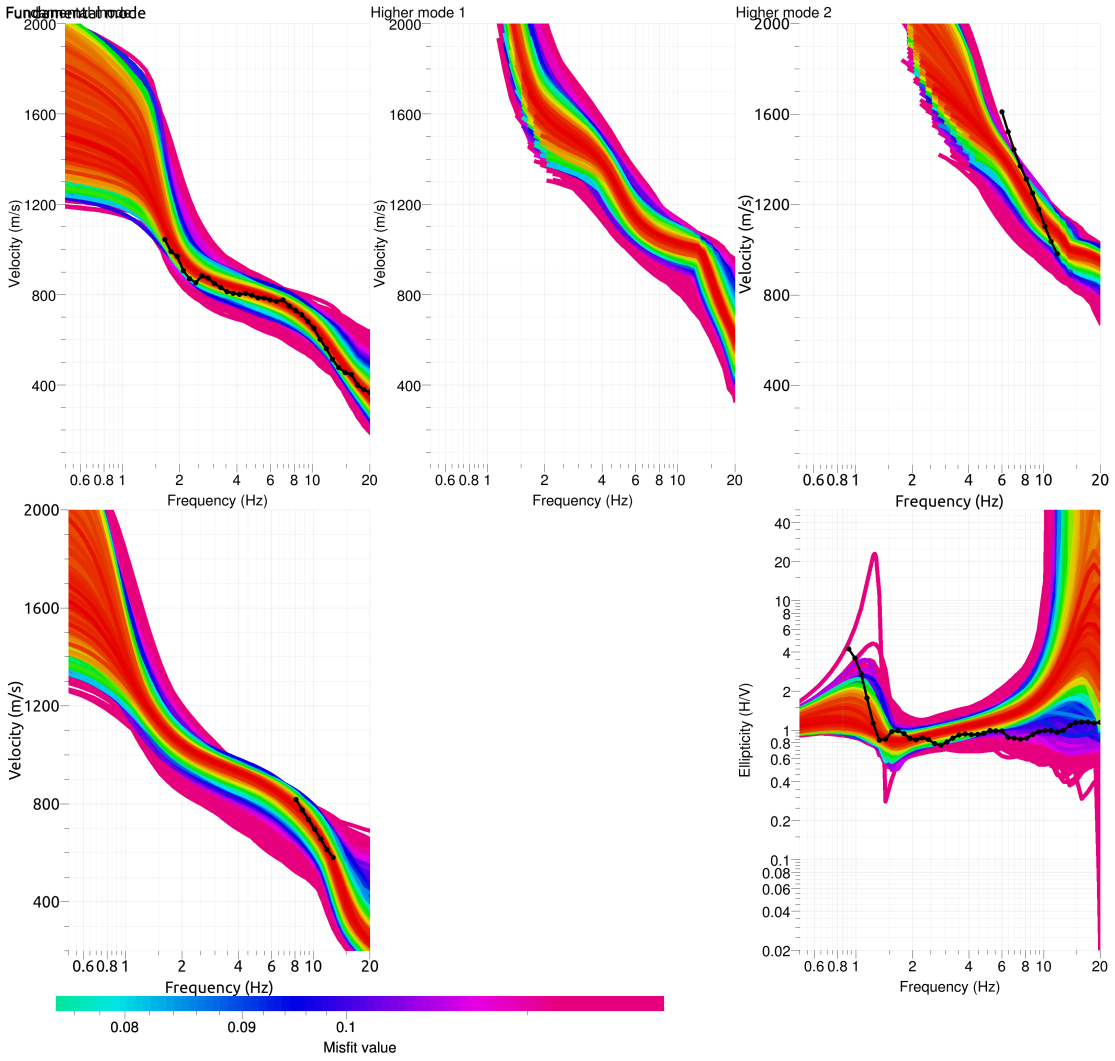

Figure 14: Comparison between inverted models and measured Rayleigh and Love modes and corresponding ellipticity, fixed layer depth strategy.

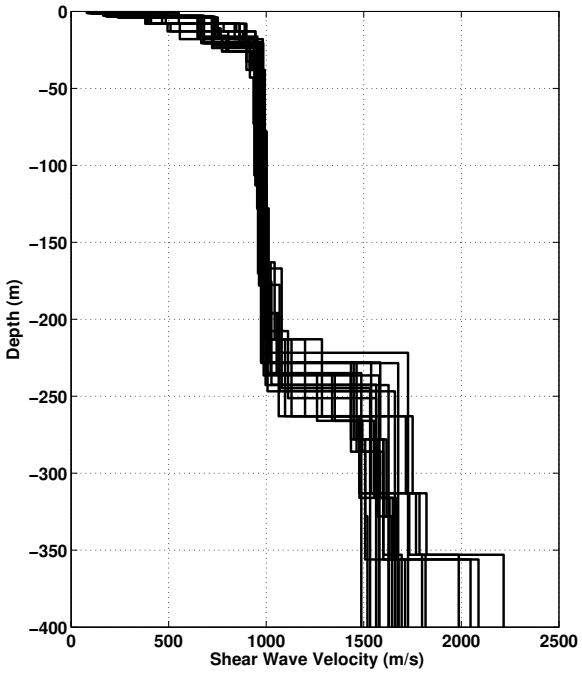

Figure 15: V_s ground profiles for the selected 25 best models.

6.2 Travel time average velocities and ground type

The distribution of the travel time average velocities at different depths was computed from the selected models. The uncertainty, computed as the standard deviation of the distribution of travel time average velocities for the considered models, is also provided, but its meaning is doubtful. $V_{s,30}$ is found to be $570\,\mathrm{m/s}$, meaning the site can be classified as class B in the Eurocode 8 [CEN, 2004] and SIA261 [SIA, 2003].

6.3 SH transfer function and quarter-wavelength velocity

The quarter-wavelength velocity approach [Joyner et al., 1981] provides, for a given frequency, the average velocity at a depth corresponding to 1/4 of the wavelength of interest. It is useful to identify the frequency limits of the experimental data (minimum frequency in dispersion curves, $1.7\,\mathrm{Hz}$ here). The results using this proxy show that no data is controlling the results below $120\,\mathrm{m}$ (Fig. 16). It seems however that the contrast around $250\,\mathrm{m}$ is constrained in the data even though the scatter is large. Moreover, the quarter wavelength impedance-contrast introduced by Poggi et al. [2012] is also displayed in the figure. It corresponds to the ratio between two quarter-wavelength average velocities, respectively from the top and the bottom part of the velocity profile, at a given frequency [Poggi et al., 2012]. It shows a trough (inverse shows a peak) at the resonance frequency.
Moreover, the theoretical SH-wave transfer function for vertical propagation [Roesset, 1970]

	Mean (m/s)	**Uncertainty (m/s)**
$V_{s,5}$	245	12
$V_{s,10}$	349	19
$V_{s,20}$	477	12
$V_{s,30}$	567	12
$V_{s,40}$	631	11
$V_{s,50}$	677	11
$V_{s,100}$	796	9
$V_{s,150}$	849	8
$V_{s,200}$	882	8

Table 7: Travel time averages at different depths from the inverted models. Uncertainty is given as one standard deviation from the selected profiles.

is computed from the inverted profiles. It is compared to the quarter-wavelength amplification [Joyner et al., 1981], that however cannot take resonances into account (Fig. 17). In this case, the models are predicting a slight amplification at the 1D resonance frequencies of the site (1, 3, 5 and $7\,\mathrm{Hz}$) increasing with frequency up to a factor of 5 around $15\,\mathrm{Hz}$. This will be compared to observations at this station.

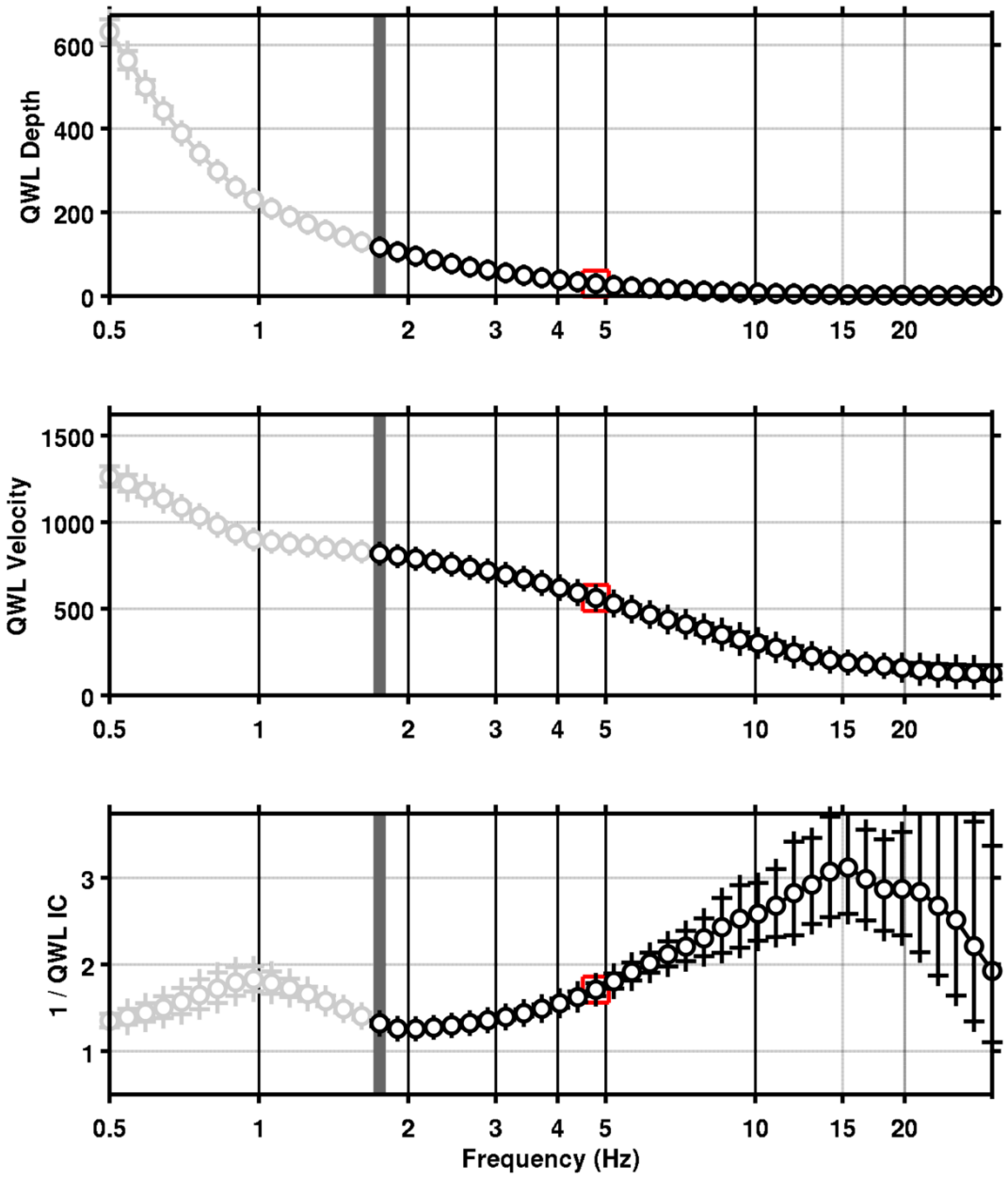

Figure 16: Quarter wavelength velocity representation of the velocity profile (top: depth, centre: velocity, bottom: inverse of the impedance contrast). Black curve is constrained by the dispersion curves, light grey is not constrained by the data. Red square is corresponding to $V_{s,30}$.

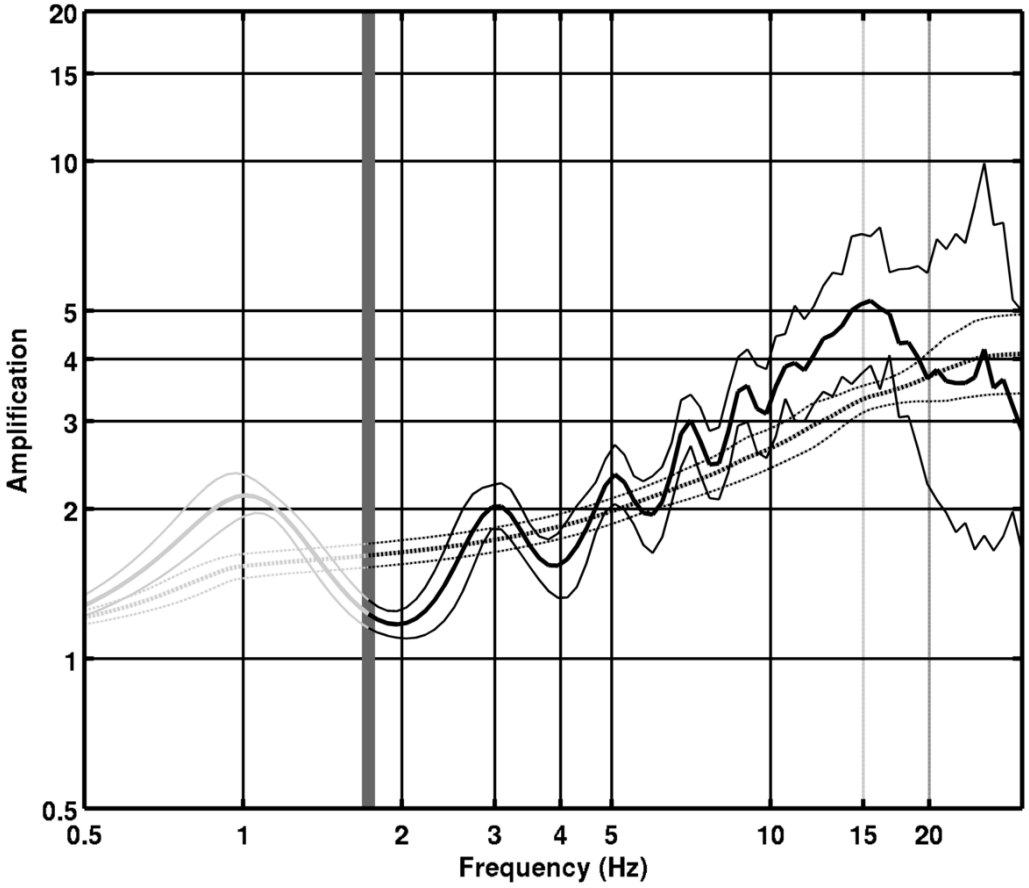

Figure 17: Theoretical SH transfer function (solid line) and quarter wavelength impedance contrast (dashed line) with their standard deviation. Significance of the greyshades is detailed in Fig. 16.

7 Conclusions

The single station measurements showed a weak 2D behaviour of the Dranse valley in Martigny with a fundamental frequency at $0.85\,\mathrm{Hz}$. Therefore, the ellipticity information could not be used in the array analysis. The array measurements presented in this study were successful in deriving a velocity model for the site of station SMAO in Martigny. We found only $3\,\mathrm{m}$ of soft sediments, variable across the array, on top on highly consolidated sediments ($700\,\mathrm{m/s}$ at $20\,\mathrm{m}$ and $1000\,\mathrm{m/s}$ at $200\,\mathrm{m}$). An interface around $250\,\mathrm{m}$ was found (velocity above $1500\,\mathrm{m/s}$) but it cannot be assured that is corresponds to the bedrock that could be even deeper considering the geological and geomorphological indications. $V_{s,30}$ is at $570\,\mathrm{m/s}$. The ground type is B for EC8 and SIA261. The theoretical SH transfer function and impedance contrast of the quarter-wavelength velocity computed from the inverted profiles show moderate amplifications at low frequencies increasing with frequency up to a factor of 5 at high frequencies. Recordings of the new station will allow to validate these simple models.

Acknowledgements

The authors thank Mrs Gay et Mabillard who allowed these measurements.

References

Sylvette Bonnefoy-Claudet, Fabrice Cotton, and Pierre-Yves Bard. The nature of noise wavefield and its applications for site effects studies. *Earth-Science Reviews*, 79(3-4): 205–227, December 2006. ISSN 00128252. doi: 10.1016/j.earscirev.2006.07.004. URL http://linkinghub.elsevier.com/retrieve/pii/S0012825206001012.

Jan Burjánek, Gabriela Gassner-Stamm, Valerio Poggi, Jeffrey R. Moore, and Donat Fäh. Ambient vibration analysis of an unstable mountain slope. *Geophysical Journal International*, 180(2):820–828, February 2010. ISSN 0956540X. doi: 10.1111/j.1365-246X.2009.04451.x. URL http://doi.wiley.com/10.1111/j.1365-246X.2009.04451.x.

J. Capon. High-Resolution Frequency-Wavenumber Spectrum Analysis. *Proceedings of the IEEE*, 57(8):1408–1418, 1969.

CEN. *Eurocode 8: Design of structures for earthquake resistance - Part 1: General rules, seismic actions and rules for buildings*. European Committee for Standardization, en 1998-1: edition, 2004.

Donat Fäh, Fortunat Kind, and Domenico Giardini. A theoretical investigation of average H / V ratios. *Geophysical Journal International*, 145:535–549, 2001.

Donat Fäh, Gabriela Stamm, and Hans-Balder Havenith. Analysis of three-component ambient vibration array measurements. *Geophysical Journal International*, 172(1):199–213, January 2008. ISSN 0956540X. doi: 10.1111/j.1365-246X.2007.03625.x. URL http://doi.wiley.com/10.1111/j.1365-246X.2007.03625.x.

Donat Fäh, Marc Wathelet, Miriam Kristekova, Hans-Balder Havenith, Brigitte Endrun, Gabriela Stamm, Valerio Poggi, Jan Burjanek, and Cécile Cornou. Using Ellipticity Information for Site Characterisation Using Ellipticity Information for Site Characterisation. Technical report, NERIES JRA4 Task B2, 2009.

William B. Joyner, Richard E. Warrick, and Thomas E. Fumal. The effect of Quaternary alluvium on strong ground motion in the Coyote Lake, California, earthquake of 1979. *Bulletin of the Seismological Society of America*, 71(4):1333–1349, 1981.

Katsuaki Konno and Tatsuo Ohmachi. Ground-Motion Characteristics Estimated from Spectral Ratio between Horizontal and Vertical Components of Microtremor. *Bulletin of the Seismological Society of America*, 88(1):228–241, 1998.

Stefano Maranò, C. Reller, H.-A. Loeliger, and Donat Fäh. Seismic waves estimation and wave field decomposition: Application to ambient vibrations. *Geophysical Journal International*, submitted, 2012.

Valerio Poggi and Donat Fäh. Estimating Rayleigh wave particle motion from three-component array analysis of ambient vibrations. *Geophysical Journal International*, 180(1):251–267, January 2010. ISSN 0956540X. doi: 10.1111/j.1365-246X.2009.04402.x. URL http://doi.wiley.com/10.1111/j.1365-246X.2009.04402.x.

Valerio Poggi, Benjamin Edwards, and D. Fah. Characterizing the Vertical-to-Horizontal Ratio of Ground Motion at Soft-Sediment Sites. *Bulletin of the Seismological Society of America*, 102(6):2741–2756, December 2012. ISSN 0037-1106. doi: 10.1785/0120120039. URL http://www.bssaonline.org/cgi/doi/10.1785/0120120039.

J.M. Roesset. Fundamentals of soil amplification. In R. J. Hansen, editor, *Seismic Design for Nuclear Power Plants*, pages 183–244. M.I.T. Press, Cambridge, Mass., 1970. ISBN 978-0-262-08041-5. URL http://mitpress.mit.edu/catalog/item/default.asp?ttype=2\&tid=5998.

Daniel Roten. *Site effects in the Rhone valley analysed by ambient noise, weak motion records and numerical simulations*. PhD thesis, ETH Zürich, 2007.

Daniel Roten, Donat Fäh, K. B. Olsen, and Domenico Giardini. A comparison of observed and simulated site response in the Rhône valley. *Geophysical Journal International*, 173 (3):958–978, June 2008. ISSN 0956540X. doi: 10.1111/j.1365-246X.2008.03774.x. URL http://doi.wiley.com/10.1111/j.1365-246X.2008.03774.x.

SIA. *SIA 261 Actions sur les structures porteuses*. Société suisse des ingénieurs et des architectes, Zürich, sia 261:20 edition, 2003.

Marc Wathelet. An improved neighborhood algorithm: Parameter conditions and dynamic scaling. *Geophysical Research Letters*, 35(9):1–5, May 2008. ISSN 0094-8276. doi: 10.1029/2008GL033256. URL http://www.agu.org/pubs/crossref/2008/2008GL033256.shtml.